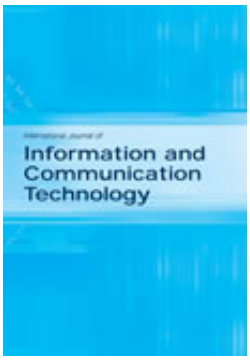

International Journal of Information and Communication Technology

ISSN online: 1741-8070 - ISSN print: 1466-6642
https://www.inderscience.com/ijict

Multi-spectral remote sensing image land classification algorithm for unmanned aerial vehicles targeting transmission line corridors

Chuntian Ma, Dan Li, Wei Hu, Weidong Liu, Guozhu Yang, Heping Wang

DOI: 10.1504/IJICT.2025.10073925

Article History:

Received:	02 July 2025
Last revised:	18 August 2025
Accepted:	18 August 2025
Published online:	22 October 2025

Multi-spectral remote sensing image land classification algorithm for unmanned aerial vehicles targeting transmission line corridors

Chuntian Ma*, Dan Li, Wei Hu, Weidong Liu, Guozhu Yang and Heping Wang

State Grid Electric Power Space Technology Company Limited, Beijing, 102211, China
Email: gwdlmct@163.com
Email: 14747428342@163.com
Email: huwei625@163.com
Email: 18611026200@163.com
Email: gzyang3912@163.com
Email: 18611026281@163.com
*Corresponding author

Abstract: Based on unmanned aerial vehicle multispectral remote sensing technology, this paper proposes a land cover classification algorithm for transmission line corridors to improve the classification accuracy and efficiency in power safety monitoring. By using drones to collect multispectral images, geometric correction is combined with median filtering and wavelet transform denoising to enhance image quality, and spectral and texture features are extracted. A multi-level segmentation system is constructed and classification thresholds are set. A convolutional neural network (CNN) with Softmax classifier and N-P criterion is used to achieve accurate land cover classification. After using the method proposed in this article to classify ground objects in multispectral remote sensing images, the F1 value is as high as 0.97 and the AUC value is as high as 0.936, indicating high classification accuracy and high effectiveness and application performance.

Keywords: transmission line corridor; land cover classification; UAV; multi-spectral remote sensing; convolutional neural network; CNN.

Reference to this paper should be made as follows: Ma, C., Li, D., Hu, W., Liu, W., Yang, G. and Wang, H. (2025) 'Multi-spectral remote sensing image land classification algorithm for unmanned aerial vehicles targeting transmission line corridors', *Int. J. Information and Communication Technology*, Vol. 26, No. 38, pp.22–41.

Biographical notes: Chuntian Ma is a technical expert in power grid surveying and mapping at State Grid Electric Power Space Technology Co., Ltd. He has long been committed to the innovative application of aerial remote sensing technology in intelligent inspection and safe operation and maintenance of transmission lines. He has participated in or presided over five scientific and technological research projects at or above the provincial level of the State Grid, obtained six national invention patents and nine utility model patents, and published ten professional papers. He has won two industry-level awards and four provincial company-level awards. Currently, he mainly focuses on the technical research of integrating aerial remote sensing technology with artificial intelligence technology in the safe operation of power grids.

Dan Li is a full-time specialist in the Aerial Remote Sensing Division of the Technical Center at State Grid Electric Power Space Technology Co., Ltd. She is mainly engaged in research on innovative technologies that integrate aerial remote sensing technology with artificial intelligence in the safe operation of power grids. She has participated in one scientific and technological research project of a provincial-level company under the State Grid, and the results have been appraised as reaching the international advanced level overall. As a key compiler, she has participated in the formulation of two internal control standards, published one professional paper, and has five invention patents under application.

Wei Hu is the Deputy Director of the Aerial Remote Sensing Division in the Technical Center of State Grid Electric Power Space Technology Co., Ltd. He has long been engaged in research on laser scanning power operation and maintenance technology for transmission lines and power space technology. As a key compiler, he has participated in the formulation of two industry standards, one group standard, five enterprise standards, and compiled one company-level manual.

Weidong Liu is Director of the Technical Center of State Grid Electric Power Space Technology Co., Ltd. and a professor-level senior engineer in electrical engineering technology. He has long been engaged in research on key technologies such as helicopter power operation technology, power transmission and transformation engineering construction technology, condition monitoring and intelligent inspection of power transmission and transformation equipment, as well as supporting technologies for operation and management of power transmission and transformation equipment. He has presided over the drafting of three power industry standards, one civil aviation industry standard, and multiple enterprise standards of the State Grid Corporation.

Guozhu Yang is a registered surveyor and the Deputy Director of the Aerospace Technology Division of State Grid Space Technology Co., Ltd. He has long been committed to the research and application of power grid space technology and digital power grid technology. He has won five provincial and ministerial level awards, obtained 19 authorised invention patents and 28 utility model patents, and received ten provincial, ministerial and industry-level awards. He has published more than 21 papers in core journals and above, and formulated two industry standards.

Heping Wang is a third-level staff member of the Science and Technology Information Department of State Grid Electric Power Space Technology Co., Ltd. He is mainly engaged in the research and application of laser scanning technology in helicopter power operations and transmission line operation and maintenance related technologies. He has been responsible for and implemented more than ten state grid science and technology projects and self-built science and technology projects of State Grid General Aviation Company. He has won the Science and Technology Progress Award from the Beijing Municipal Government, China Surveying and Mapping Association and State Grid Corporation of China for many times.

1 Introduction

Transmission line corridors often span complex terrains such as mountains, hills, plains, and rivers, as well as diverse environments such as cities, rural areas, forests, and farmland. The geographical differences are significant, and natural and human factors are intertwined, making the line corridors face many potential safety threats (Tarolli et al., 2021). For example, in densely forested areas, the rapid growth of trees may gradually approach power transmission lines, causing tree line discharge accidents; in addition, force majeure factors such as geological disasters and severe weather may also cause damage to the railway corridor. Manual inspection not only consumes a lot of manpower, material resources, and time costs, but is also limited by the physical fitness, experience, and working environment of the inspection personnel, making it difficult to achieve comprehensive and timely inspection of the line corridor (Zheng et al., 2024). In this context, the rise of unmanned aerial vehicle multi-spectral remote sensing technology has brought revolutionary changes to the ground monitoring of transmission line corridors. Images can capture the spectral reflectance characteristics of land cover in different bands, containing rich information about land cover. By analysing and processing this spectral information, accurate identification of land cover types, growth conditions, spatial distribution, etc. can be achieved (Ma et al., 2022). Drones, with their advantages of flexible manoeuvrability, low cost, and rapid deployment, can be equipped with multi-spectral sensors to efficiently and comprehensively inspect transmission line corridors, and timely obtain information on land changes. This technology can help the power industry monitor the dynamic changes of transmission lines in real time, significantly improving the reliability of power supply (Li et al., 2025a).

Many researchers and experts have conducted in-depth research on this. Wang et al. (2025) designed a hyperspectral and multi-spectral remote sensing image classification method by combining mixed convolution and cascaded group attention mechanism. By using self attention mechanism to capture global dependencies in images, combined with the local feature extraction ability of CNN, the 3D EfficientViT module in the convolutional network structure achieves high-precision classification of Images. However, the computational complexity of the self attention mechanism is directly proportional to the square of the sequence length, which leads to a decrease in performance and a lack of sufficient generalisation ability when dealing with long sequences or high-resolution images in different scenes or resolutions. Fan et al. (2025) fused the features of LiDAR data and hyperspectral remote sensing images, constructed a multimodal cross feature fusion module, and integrated multi-scale semantic information from multiple sources of data through a composite granularity feature integration module, achieving effective classification of remote sensing images. However, the cross feature granularity fusion network used may include multiple complex modules, such as multimodal cross feature fusion module and composite granularity feature integration module. If the quantity or quality of training samples is insufficient, it may affect the classification performance of the model in practical applications. Haider et al. (2025) designed a lightweight remote sensing image classification method based on convolutional neural networks (CNNs). Five different neural network classifiers were introduced into the original CNN, and through continuous optimisation of the model architecture and the combination of classifiers, it was ultimately determined that the wide NN classifier and medium NN classifier have better application performance in remote sensing image classification tasks. Although wide NN and medium NN classifiers have

performed well in experiments, lightweighting often comes at the cost of sacrificing classification accuracy. Further evaluation is needed to determine whether lightweight models can meet the requirements of classification accuracy while maintaining real-time performance, especially when dealing with complex scenes or high-resolution images.

Therefore, this article uses drones to collect multi-spectral remote sensing images and designs a method for classifying ground objects in transmission line corridors.

2 Remote sensing image object classification method design

2.1 Remote sensing image acquisition

The scope of construction for transmission line corridors is relatively large, encompassing elements such as transmission line towers, conductors, vegetation, roads, and buildings. Through targeted image acquisition, detailed land cover information in the area can be obtained. This provides accurate and relevant data support for subsequent land cover classification and makes the classification results more in line with the actual situation of the transmission line corridor. The image acquisition effect directly and profoundly affects the construction accuracy and texture fit of subsequent 3D models, and is one of the key factors determining the quality of 3D models (Yang et al., 2025a). Given the diverse forms and complex structures of land features in complex areas, a multi-viewpoint acquisition strategy is usually required to ensure that each part can be accurately captured and presented in its entirety. Specifically, at least three viewpoints that are close to each other but have different perspectives should be selected for remote sensing image acquisition. This multi-viewpoint collection method can obtain rich information about land features from different angles, providing more comprehensive and detailed data support for subsequent 3D reconstruction. At the same time, in order to ensure accurate matching and seamless stitching of multi-spectral remote sensing images in three-dimensional space, and thereby improve the integrity and accuracy of three-dimensional models, it is necessary to ensure a high proportion of overlap between continuously collected images (Sun et al., 2025). A high proportion of overlap means that there are a large number of identical feature points between adjacent images, which can serve as important basis for image matching and stitching, effectively reducing stitching errors and improving the spatial consistency and geometric accuracy of the 3D model.

Choose a drone with appropriate flight altitude, speed, and endurance. The flight altitude needs to be determined based on the image resolution requirements and the terrain characteristics of the transmission line corridor area to ensure that the obtained images can clearly reflect the details of the terrain (Qi et al., 2025). It is possible to plan the navigation area for drone image acquisition and calibrate the flight altitude to meet the requirements of high-resolution acquisition. The calculation formula is as follows:

$$H \times \alpha = f \times GSD \tag{1}$$

In the formula, H is the flight altitude of the drone; f is the focal length of the onboard camera; α is the pixel size; GSD is the ground sampling distance.

Images that do not meet the requirements need to be re captured for smooth image processing, stitching, and analysis in the future. After importing multi-spectral remote

sensing images into Smart3D software, multi-spectral remote sensing images that meet the accuracy requirements are obtained:

$$I = u \times f \times a(b \times s) \tag{2}$$

In the formula, u represents the accuracy of multi-spectral remote sensing image acquisition; a is the maximum pixel of multi-spectral remote sensing images; b and s are the sensor width and camera distance, respectively.

2.2 Multi-spectral remote sensing image correction of transmission line corridors

Due to various factors such as sensor performance, changes in flight attitude, and Earth's curvature, geometric distortion occurs in the images. The core goal of geometric correction is to eliminate these distortions and ensure that geographic features in the image accurately match their true spatial positions on the ground. This process is critically important for key tasks such as information extraction and image analysis. If remote sensing images are not geometrically corrected, the extracted boundaries of land use types within transmission line corridors will likely deviate significantly from the actual boundaries, resulting in inaccurate planning outcomes. Therefore, it is necessary to perform geometric correction on the collected images to ensure the correctness of ground object position information and provide reliable data support for the classification of ground objects in subsequent transmission lines (Zheng et al., 2025).

Set $p(x, y)$ as any point on the original image, (x, y) as the image point, and $D(x, y)$ as the point on the corrected image. There is a one-to-one mapping relationship between the two points, which can be expressed in the following form:

$$\begin{aligned} p(x, y)&\begin{cases} x = f_x(x, y) \\ y = f_y(x, y) \end{cases} \\ D(x, y)&\begin{cases} x = \varphi_x(x, y) \\ y = \varphi_y(x, y) \end{cases} \end{aligned} \tag{3}$$

In the formula, $\varphi_x(x, y)$ and $\varphi_y(x, y)$ are the mapping functions of the original image points (x, y); $f_x(x, y)$ and $f_y(x, y)$ are the mapping functions of (x, y) points in the corrected image.

The distortion difference mainly comes from factors such as the internal orientation element error of digital cameras, optical system distortion, and deformation of area sensors. These distortions can cause deviations between the captured image and the real scene, therefore, it is necessary to correct the camera distortion problem. The camera distortion correction model is described by the following equation:

$$\begin{cases} \Delta x = (x - x_0)(l_1 r^2 + l_2 r^4) \\ \Delta y = (y - y_0)(l_1 r^2 + l_2 r^4) \end{cases} \tag{4}$$

$$I(\Delta x, \Delta y) = \left[D(x, y) - l_1 l_2(x, y) \right] \tag{5}$$

In the formula, r is the radial distance from the image point (x, y) to the image principal point (x_0, y_0); Δx and Δy represents the correction values in the x and y directions,

respectively; l_1 and l_2 are radial distortion factors, respectively; I is the corrected multi-spectral remote sensing image.

2.3 Image denoising

The collection of remote sensing images is inevitably affected by various factors, resulting in some noise. These noises can significantly reduce image quality and have adverse effects on subsequent image analysis and information extraction work (Wang et al., 2024). Therefore, further denoising processing is needed for the image.

Median filtering is a nonlinear filtering method that can quickly and accurately identify and remove these noise points, while preserving the edges and details of the image to the greatest extent possible (Liu et al., 2025). For example, in details such as the edges of transmission lines and the contours of towers in images, median filtering can maintain their clarity while denoising, avoiding edge blurring caused by denoising processing. In the multi-spectral remote sensing images of unmanned aerial vehicles in transmission line corridors, different land features and details have different spatial frequency characteristics (Liu et al., 2023). The multi-scale analysis capability of wavelet transform enables targeted processing based on the characteristics of information at different scales. For example, the texture information of transmission lines can be preserved and enhanced at an appropriate scale; for noise, it can be suppressed in high-frequency components to achieve fine denoising and feature extraction of the image. Therefore, this article adopts a denoising method combining median filtering and wavelet transform to process images.

Step 1 Transform the noisy remote sensing image with two-dimensional wavelet transform into the wavelet domain, decompose it into three layers, and obtain the images of each sub-band after decomposing it into three layers.

Step 2 Filter the low-frequency sub transmission line corridor multi-spectral remote sensing image after wavelet transform using the neighbourhood averaging method, so that the greyscale value of pixel w in the transmission line corridor image is $W(j, k)$, where j and k represent the average pixel values in the horizontal and vertical directions of the window pixels, respectively; the set of window pixels is A, with N pixels in A. Using $W(j, k)$ as the centre, the neighbourhood averaging method is used for filtering. The calculation formula for the window pixel mean $U(j, k)$ corresponding to pixel w is as follows:

$$U(j,k) = \frac{1}{N\eta} \sum_{(x,y)\in A} w(x, y) I(\Delta x, \Delta y) \tag{6}$$

In the formula, η is the regulatory factor.

In the process of smoothing the neighbourhood mean, the neighbourhood L is determined with the unit distance as the radius, and the formula is as follows:

$$L = \{(j-1, k-1), (j+1, k), (j, k+1), (j-1, k)\} \tag{7}$$

By using the over limit neighbourhood averaging method to process the multi-spectral remote sensing images of transmission line corridors, the degree

of blur and distortion in the multi-spectral remote sensing images of transmission line corridors can be reduced. The formula is as follows:

$$U(j,k)=\begin{cases}\dfrac{1}{N\eta}\displaystyle\sum_{(x,y)\in A} w(x,y) & \left|w(j,k)-\dfrac{1}{N\eta}\displaystyle\sum_{(x,y)\in A} w(j,k)\right|>T \\ w(j,k) & \text{else}\end{cases} \tag{8}$$

In the formula, T is the threshold.

Step 3 Median filtering of multi-spectral remote sensing images of transmission line corridors in each high-frequency sub-band, determination of pulse points through local energy $E(x, y)$, and determination of local energy thresholds for neighbouring windows.

$$T'=\frac{\beta\times\displaystyle\sum_{m=1}^{M}E_m}{\eta M}E(x,y)U(j,k) \tag{9}$$

In the formula, β is a constant; M is the total number of points in the neighbourhood; E_m is the local energy of the m^{th} point.

The condition for determining whether a point is pulse noise is $E(x, y) > T'$. If this condition is met, then the point is pulse noise and median filtering processing is required. And through adaptive wavelet thresholding, the multi-spectral remote sensing images of transmission line corridors in various high-frequency sub bands are processed (Niu et al., 2020). The formula for calculating using adaptive wavelet thresholding is as follows:

$$T''_{R,i}=C_i\eta\sigma\sqrt{\frac{2\log(R+1)}{V}}\times 2^{\frac{S(R)}{2}} \tag{10}$$

In the formula, S is the decomposition scale; R is the decomposition scale number, $R = 1, 2, \ldots, V$; σ is the standard deviation of noise; C_i is the sub-band of the i^{th} transmission line corridor multi-spectral remote sensing image.

Step 4 The wavelet soft threshold function is used to quantise the image, and its formula is as follows:

$$\begin{aligned}\lambda\left(w(j,k)\right)&=\operatorname{sgn}\left(w(j,k)\right)\left(\left|w(j,k)\right|_j-T_i''\right)_+\\&=\begin{cases}\left|w(j,k)\right|_j-T_i''; & w(j,k)_j\geq T_i''\\0; & \left|w(j,k)_j\right|<T_i''\\\left|w(j,k)\right|_j+T_i''; & w(j,k)_j\leq T_i''\end{cases}\end{aligned} \tag{11}$$

In the formula, T_i'' is the adaptive wavelet threshold of the i^{th} transmission line corridor multi-spectral remote sensing image sub-band; $\lambda(w(j, k))$ is the wavelet soft threshold function.

Step 5 Implement reasonable coefficient enhancement on the multi-spectral remote sensing images of transmission line corridors in each high-frequency sub-band after threshold quantisation, so that the multi-spectral remote sensing images of transmission line corridors meet visual requirements;

Step 6 Obtain the denoised multi-spectral remote sensing image of the transmission line corridor after wavelet inverse transform coefficient enhancement.

2.4 Extraction of spectral and texture features

In the field of remote sensing image analysis, spectral features and texture features are two key sources of information that can provide rich and complementary descriptions of land features from different dimensions (Chen et al., 2025). There are significant differences in the material composition and internal structural characteristics of different land features, which are directly reflected in their response characteristics to electromagnetic waves, manifested in different reflection and absorption characteristics in the spectral dimension (Li et al., 2025b). Based on this principle, by deeply extracting spectral features of images, such as obtaining key parameters such as reflectivity or radiance in different bands, different types of land cover can be distinguished. Therefore, after completing the denoising process of the image, the spectral and texture features of the image are extracted.

For this, this article selects the image pixel mean μ_J, spectral contribution rate R_J, and pixel standard deviation δ_J as spectral feature extraction indicators, and their specific calculation formulas are as follows.

$$\begin{cases} \mu_J = \dfrac{\sum_{h=1}^{n} v_h}{n} \\ R_J = \dfrac{\overline{C_J}}{L_{correct} \cdot \sum_{h=1} \overline{C_h}} \\ \delta_J = \sqrt{\dfrac{\sum_{h=1}^{n} (v_h - \mu_J)^2}{n-1}} \end{cases} \tag{12}$$

In the formula, n_J is the total number of bands in the image; n is the total number of image pixels; v_h is the pixel amplitude of the image; $\overline{C_J}$ is the spectral value; $\overline{C_h}$ is the total spectrum of the image; $L_{correct}$ is radiance.

Using homogeneity *HOMO*, contrast *CON*, and texture entropy *ENT* as indicators for extracting image texture features. Assuming that in the grey level co-occurrence matrix of the image, (c, d) represents the position of the current element in the row and column, and B represents the total number of rows and columns, the expression for texture feature extraction is as follows.

$$\begin{cases} HOMO = \sum_{c,d=0}^{B-1} \frac{P_{c,d}}{1+(c-d)^2} \\ CON = \sum_{c,d=0}^{B-1} P_{c,d} \cdot (c-d)^2 \\ ENT = \sum_{c,d=0}^{B-1} P_{c,d} \cdot \left(\ln P_{c,d}\right) \end{cases} \tag{13}$$

In the formula, $P_{c,d}$ represents the corresponding pixel value at position (c, d).

The above content can effectively extract spectral and texture features from multi-spectral remote sensing images of transmission line corridors.

2.5 Hierarchical extraction of land cover information

Different land features have unique reflection and absorption characteristics in the spectrum. For example, vegetation usually has a higher reflectivity in the near-infrared band, while water has a lower reflectivity in the near-infrared band. By extracting spectral features such as reflectance or radiance in different bands, different types of land cover can be preliminarily distinguished. And texture reflects the spatial structure information of the surface of the ground object. For example, forest land usually has complex textures, while cultivated land may exhibit regular ridge textures. Texture features can supplement the shortcomings of spectral features in distinguishing similar land features. The combination of the two can more comprehensively describe the characteristics of land features and improve the accuracy of classification. Different features in the transmission line corridor have different spatial scales. Roads usually have a relatively regular elongated structure, with relatively small and uniform scales; forest land often has a large area, complex internal structure, and large scale; farmland and grassland have different scales depending on planting or growth conditions. Single scale segmentation is difficult to adapt to the characteristics of all land features. By constructing multiple segmentation levels, more suitable segmentation can be performed for land features of different scales (Yang et al., 2025b).

Therefore, after extracting spectral and texture features, a multi-level segmentation system can be constructed based on these features and the principle of scale segmentation. Construct four segmentation levels at different scales, targeting road information, forest information, cultivated land information, and grassland information contained in multi-spectral remote sensing images. Design extraction rules that are adapted to each type of terrain information, and achieve accurate classification of terrain information in transmission line corridors through this layered extraction method.

Roads, forests, cultivated land, and grasslands have their own unique characteristics. Roads usually have obvious linear characteristics and high reflectivity contrast; forest land has rich vegetation spectral characteristics and complex textures; farmland may have regular planting patterns and specific spectral responses; grasslands have relatively uniform spectral and texture features (Liu, 2024). Designing specialised extraction rules for different land features can fully utilise these characteristics and improve the accuracy of extraction. The hierarchical extraction structure of specific terrain information is shown in Figure 1.

Figure 1 Hierarchical extraction structure of land cover information

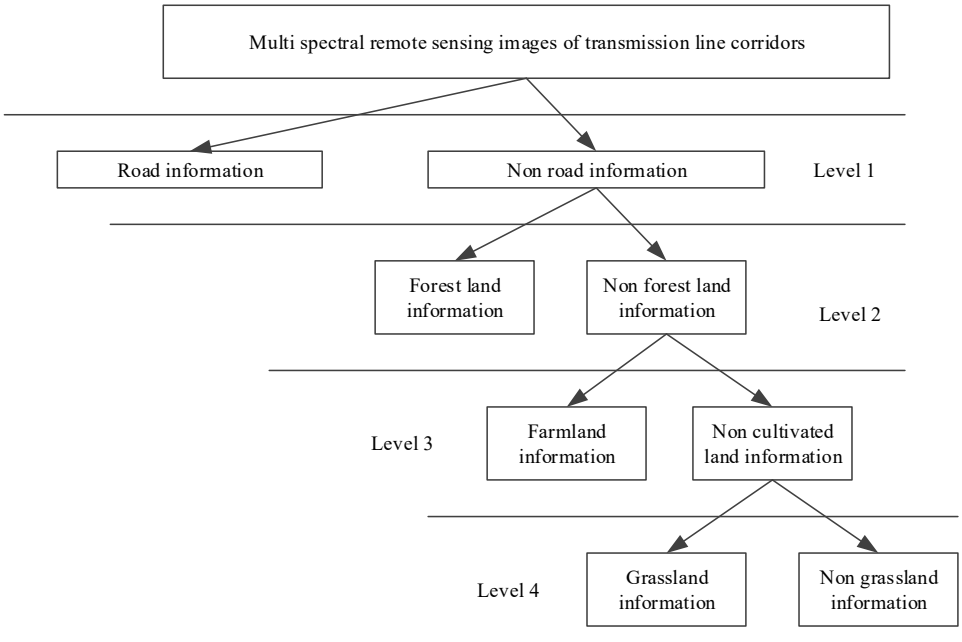

Considering the similarity between forest land and cultivated land in images, in order to optimise the information extraction effect, this paper introduces the near-infrared ratio *ratio* parameter to distinguish similar forest land and cultivated land. The specific calculation formula is shown below.

$$ratio = \frac{v_h(K)}{\sum_{h=1}^{n} v_h(K)} \tag{14}$$

In the formula, $v_h(K)$ represents the greyscale mean of pixels in a specific multi-spectral remote sensing image layer. For grassland information, this article uses the normalised vegetation index *NDVI* as the extraction threshold, and its specific expression is as follows.

$$NDVI = \frac{NIR - red}{NIR + red} \tag{15}$$

In the formula, *NIR* represents the reflectance in the near-infrared band, and *red* represents the reflectance in the red band. Based on the above indicators, the hierarchical extraction rules for land cover information constructed in this article are shown in Table 1.

Based on Table 1, a hierarchical extraction rule for ground information in multi-spectral remote sensing images of transmission line corridors can be constructed. By setting extraction thresholds for different feature indicators, different ground information can be extracted in layers.

Table 1 Rules for hierarchical extraction of land feature information

Extract hierarchy	*Spectral characteristic indicators*	*Texture feature indicators*	*Other indicators*
Road information	$\delta_J \leq 0.154$	$CON \geq 0.214$	$NDVI \leq 0.024$
Forest land information	$\mu_J \leq 0.08$	$CON \leq 0.175$	$NDVI \geq 0.845$
			$ratio \leq 0.21$
Farmland information	$R_J \geq 0.742$	$HOMO \geq 0.753$	$NDVI \leq 0.382$
Grassland information	$R_J \leq 0.718$	$ENT \geq 0.21$	$NDVI \geq 0.345$

2.6 Land cover classification based on CNN

Due to the differences in spectral and spatial information, each land type has unique spectral reflection characteristics and spatial texture structures, manifested as complexity and diversity. Traditional methods are difficult to fully explore these deep level features to achieve accurate classification (Pacheco and de Andrade, 2024). Based on this, after extracting different terrain information in layers, CNNs are introduced for terrain classification. CNN, with its unique convolution mechanism, can efficiently extract features of land cover information from local areas of input remote sensing image data (Gou et al., 2025). Through layer by layer convolution and pooling operations, more discriminative features are gradually abstracted, thus better capturing subtle differences between different categories of land cover information in the image and laying a solid foundation for high-precision land cover classification (Zhang et al., 2025). Moreover, the feature of the filters in the convolutional layer sharing weights across the entire input image greatly reduces the number of parameters in the network, effectively avoiding the risk of overfitting caused by too many parameters and significantly improving the generalisation ability of the model, enabling it to maintain stable classification performance when facing multi-spectral remote sensing images of transmission line corridors in different scenarios and conditions (Wei et al., 2022). At the same time, this feature can effectively reduce misjudgments or even omissions in the classification process, minimise classification losses, and provide reliable technical support for precise monitoring and management of transmission line corridors.

The application of softmax classifier in CNN is quite common (Turner et al., 2022). In the complex scenario of transmission line corridors, there are many interference factors, such as vegetation changes in different seasons, differences in lighting conditions, and the interweaving of various land features, making the scene extremely complex. The softmax classifier, with its unique advantages, can adapt well to such complex environments. It not only has strong multi-classification support capabilities, but also can accurately distinguish various land types such as conductors, vegetation, farmland, roads, etc. in transmission line corridors. Moreover, its calculation process is relatively simple and efficient, which can quickly process a large amount of remote sensing image data while ensuring classification accuracy (Tan et al., 2025). Therefore, the softmax classifier is selected to assist in detecting anomalies related to scale perception in transmission line corridor scenes, providing strong technical support for the safe operation monitoring of transmission line corridors.

In multi-classification, assuming γ is the total number of land cover categories in remote sensing images, and inputting the invariant moment feature $Z_X = \{\phi_1, \phi_2, \ldots, \phi_X\}$

obtained in the previous section, the probability of all classification output results can appear, that is, the input $Z_X = \{\phi_1, \phi_2, \ldots, \phi_X\}$, and the probability value G_Y of $Q(O = Y|Z_X)$ is estimated based on the Y ($Y = 1, 2, \ldots, \gamma$) category.

$$G_Y(Z_X) = \begin{bmatrix} Q(O_X = 1|Z_X;\theta) \\ Q(O_X = 2|Z_X;\theta) \\ \cdots \\ Q(O_X = \gamma|Z_X;\theta) \end{bmatrix} \tag{16}$$

In the formula, θ is the parameter trained by CNN.

In classification tasks, the accuracy of classification is closely related to the probability values of selecting each category, and the two are directly proportional. This means that the higher the probability of a category being selected, the greater the likelihood of the classification result being correct (Yu et al., 2024). However, in practical operation, if there are errors in adjusting network parameters, or if the extracted sample feature points are not complete and comprehensive enough, it is easy for the classifier to make incorrect judgments, resulting in misjudgments. In the output layer of classification models such as CNNs, a probability value is calculated for each category. When the probability value of category Y is the highest among all categories, the classifier will determine the final classification result as category Y. From a theoretical perspective, this decision method based on maximum probability can improve the accuracy of classification to a certain extent and avoid classifier misjudgment to the greatest extent possible.

Figure 2 Multi-layer CNN structure diagram (see online version for colours)

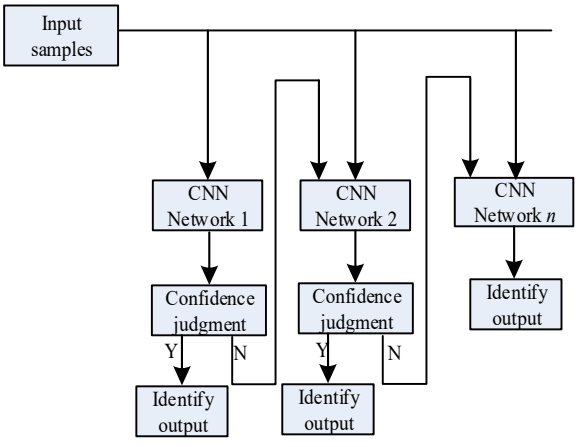

But in order to further reduce the misjudgment rate, the concept of confidence judgment function was introduced. This function will perform detailed recognition and judgment based on the information output by the sample. Specifically, for each sample, the confidence judgment function evaluates whether it meets the predetermined judgment conditions (Fayaz et al., 2025). If the sample does not meet the judgment criteria, it indicates that the current classification result may not be reliable enough, and the sample will enter the next layer of the network for further processing and analysis; on the

contrary, if the sample meets the judgment criteria, it indicates that the current classification result has high credibility, and the classifier will directly recognise it and output the final result. Through this approach, the accuracy and reliability of classification can be effectively improved, reducing the occurrence of misjudgments. The structure diagram of the multi-layer CNN is shown in Figure 2.

In the classification of land features in transmission line corridors, misjudgment refers to the classification model incorrectly identifying land features that actually belong to one category as other categories. For example, identifying transmission towers as buildings or mistaking wires for vegetation. Misjudgment can lead to a biased understanding of the terrain in the transmission line corridor, which may affect subsequent maintenance, planning, and safety assessment work. And missed judgment refers to the classification model failing to recognise a certain category of land cover that actually exists, that is, the land cover of that category is missed in the classification results. For example, there is actually a small illegal building in the transmission line corridor, but the classification model failed to recognise it. Omission of judgment may result in potential issues not being detected and addressed in a timely manner, posing a threat to the safe operation of transmission lines. Therefore, in order to effectively prevent misjudgments and omissions, it is necessary to give high confidence to the ground information samples and adjust the judgment threshold accordingly to reduce the safety hazards of transmission lines.

The Naiman Pearson criterion (N-P criterion) is a decision criterion used in hypothesis testing to balance the probabilities of two types of errors. The core idea is to minimise the probability of another type of error (such as false alarm probability) or maximise the effectiveness of the test, while limiting the probability of a certain type of error (such as false alarm probability). The core of the N-P criterion is to find a test that minimises the probability ρ_V of the second type of error (false positive) given the probability ρ_F of the first type of error (false positive), or equivalently, maximises the effectiveness of the test (i.e., the probability of correctly rejecting the null hypothesis). The N-P criterion is mainly designed around the optimisation of missed judgments (type 2 errors), while constraining false judgments (type 1 errors) and determining the decision threshold μ. It is suitable for scenarios where the probability of missed judgments is minimised while controlling the probability of false judgments.

Therefore, according to the N-P criterion, the probability of misjudgment and missed judgment is calculated as follows:

$$\rho_V = \rho_F\left(\overline{Z} \le z\right) = \int_{-\infty}^{z} f(\theta)dx \tag{17}$$

In the formula, $f(.)$ is the probability density function; z is the judgment threshold.

After calculating the probability of misjudgment and missed judgment based on the N-P criterion, CNN is used to classify ground targets in the image.

It is known that the CNN model classifies the input multi-spectral remote sensing image I and outputs a probability of $G_Y(Z_X)$ for a certain category, γ for the total number of land cover categories, and G_Y for the probability that the remote sensing image belongs to the Y^{th} category. The decision threshold μ determined by the N-P criterion can be used to obtain the land cover classification results through the following classification decision rules. The calculation formula is as follows:

$$H = \begin{cases} \arg\max_X G_Y, & \text{if } \max_X G_Y \geq \mu \\ \text{Reject classification}, & \text{if } \max_X G_Y < \mu \end{cases} \tag{18}$$

In the formula, $\max_X G_Y$ is the maximum value in the category probability vector, representing the highest confidence of the CNN model that the image belongs to a certain category; $\arg\max_X G_Y$ is the category index corresponding to the maximum value in the category probability vector, which is the most likely category obtained by the CNN model classification.

By combining the decision threshold of N-P criterion with the classification ability of CNN using the above formula, the land cover classification of multi-spectral remote sensing images in transmission line corridor scenes has been achieved.

3 Experiment

3.1 Experimental setup

To verify the application performance of the unmanned aerial vehicle multi-spectral remote sensing image land classification algorithm proposed in this article, experiments were designed for testing. The research object of this experiment is selected as a typical mountainous transmission line corridor area (Figure 3), which spans complex terrain, covering high mountains, hills, and river valleys, with a total area of about 50 square kilometres, including more than 200 transmission towers and over 80 kilometres of conductor length. Forest land, farmland, grassland, and scattered residential areas are distributed along the line. The experiment requires the use of a DJI M300 multi-rotor drone equipped with a five lens multi-spectral camera, covering the visible to near-infrared wavelength range. The flight altitude is set at 120m to ensure a ground resolution of 0.2 m/pixel, and an 80% image overlap rate is achieved by planning a 'zigzag' shaped flight path.

Figure 3 Schematic diagram of the research area (see online version for colours)

In the laboratory data processing stage, Smart3D software is used for image stitching and 3D modelling. ENVI 5.3 is used to extract spectral and texture features, and a CNN model is built using the PyTorch framework. The training process is monitored using TensorBoard visualisation tool, and finally ArcGIS Pro is used for spatial analysis and accuracy verification of the classification results. This setting takes into account the adaptability to complex terrain, the integrity of multi-spectral data, and the validation requirements of deep learning algorithms, and can systematically evaluate the effectiveness of land classification algorithms in transmission line corridor scenarios.

3.2 Multi-spectral remote sensing image processing of unmanned aerial vehicles

After using drones to obtain multi-spectral remote sensing images, there may be geometric distortions in the original images. These distortions can be eliminated through geometric correction, enabling the geographic elements in the image to accurately correspond to their actual geographic spatial positions. After completing the correction process, there are still some noise points in the image, and excessive noise can affect the effectiveness of feature extraction of ground information. Therefore, the collected images can be processed by using a denoising method that combines median filtering and wavelet transform. The processing result is shown in Figure 4.

3.3 Experimental analysis

3.3.1 F1-measure

In the scenario of land cover classification, the distribution of different land cover types in unmanned aerial vehicle multi-spectral remote sensing images is often uneven, and some land cover types may belong to minority categories. If we only focus on accuracy, we may overlook the model's ability to recognise a few types of land features. The F1 measure can more comprehensively reflect the recognition effect of different methods on minority land cover, thus more accurately evaluating the comprehensive performance in practical applications. In this test, 500 multi-spectral remote sensing images were randomly selected and compared with the methods in Wang et al. (2025) and Fan et al. (2025) to detect the F1 measure of the classification results. The detection results are shown in Figure 5.

From Figure 5, it can be seen that after using the method in Wang et al. (2025) for land cover classification, the F1 measure remains stable between 0.84 and 0.89, while when using the method in Fan et al. (2025) for classification, the F1 measure range fluctuates between 0.82 and 0.93. Using the method proposed in this article for land cover classification, the F1 measure is as high as 0.95–0.97, demonstrating the highest classification accuracy. This not only means that the method can accurately identify land cover information in multi-spectral remote sensing images, but also more effectively classify different land cover types and reduce false alarm rates.

Figure 4 Multi-spectral remote sensing image processing results of unmanned aerial vehicle, (a) original multi-spectral remote sensing images (b) correction processing result (c) denoising processing result (see online version for colours)

(a)

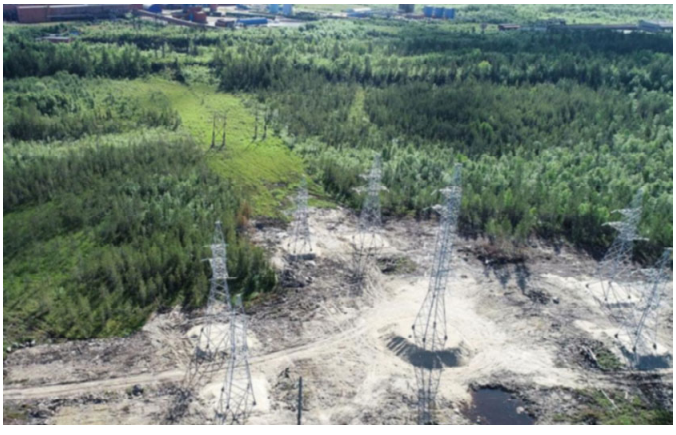

(b)

(c)

Figure 5 Comparison of F1 measure for land cover classification using different methods (see online version for colours)

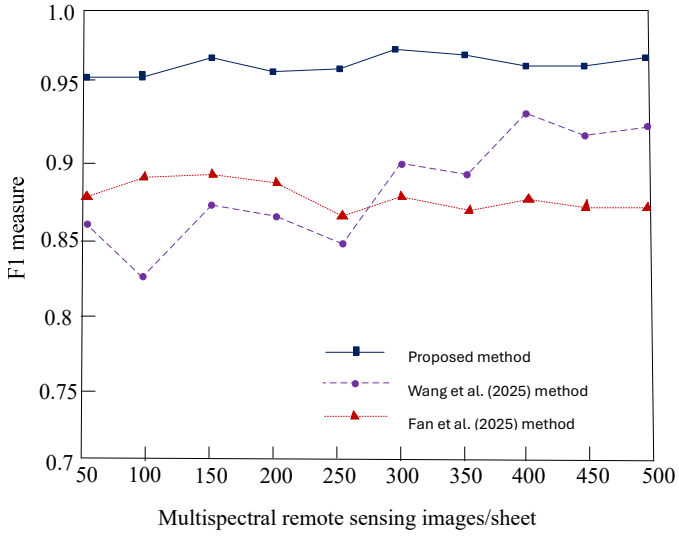

Figure 6 Comparison of ROC curves for land cover classification using different methods (see online version for colours)

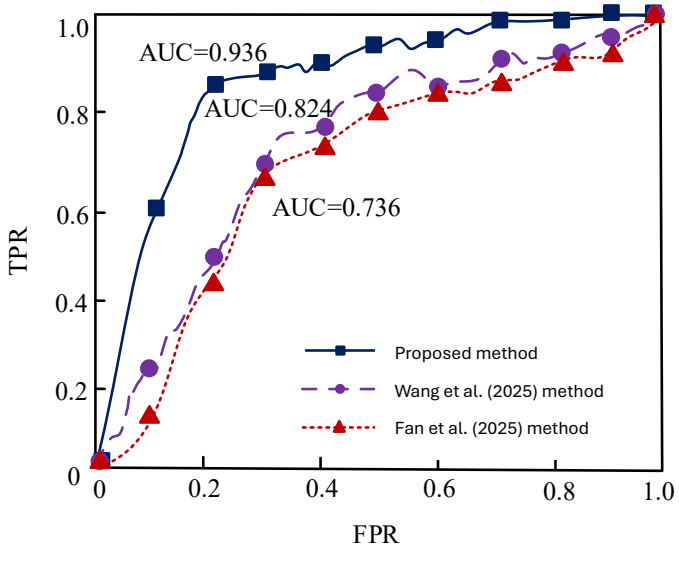

3.3.2 ROC curve

The receiver operating characteristic (ROC) curve is an important means of evaluating the classification ability of algorithms, which can intuitively reflect the overall discriminative ability of the model. Especially in scenarios where the distribution of land cover categories is uneven (such as when there are few rare land cover samples) or the

classification threshold needs to be dynamically adjusted, the ROC curve is not affected by the prior probability of the category, and can comprehensively display the performance changes of the model from conservative to aggressive strategies. The area under the curve AUC is more like the overall quality of a single numerical quantification model. The closer this value is to 1, the better the application performance of the classifier in the classification process. Compare the ROC curves of different classification methods and calculate the AUC value. The result is shown in Figure 6.

From Figure 6, it can be seen that the area under the ROC curve for land cover classification using the methods of Wang et al. (2025) and Fan et al. (2025) is relatively small, with AUC values of 0.824 and 0.736, respectively; in contrast, after using the method proposed in this article for classification, the area under the ROC curve significantly increased, and the AUC value reached 0.936, indicating a higher accuracy in classifying land cover information. It has been proven that the proposed method has good application effect in the land classification task of multi-spectral remote sensing images of unmanned aerial vehicles in transmission line corridors.

4 Conclusions

This study developed a multi-spectral remote sensing image classification method based on unmanned aerial vehicles. Leveraging drones equipped with multi-spectral sensors, we captured imagery tailored to corridor-specific geographical environments and land distribution patterns. Following geometric correction and denoising procedures, spectral and texture features were extracted. A hierarchical segmentation system was subsequently established, incorporating CNNs for precise land cover classification. Experimental validation demonstrated outstanding performance, with F1 measure of 0.95–0.97 and an AUC of 0.936 – significantly surpassing conventional approaches. Looking forward, continued advances in AI and machine learning could enable integration of UAV multi-spectral technology with internet of things and 5G systems, ultimately supporting aerial-space-ground monitoring networks for enhanced power grid safety and operational efficiency.

Declarations

Authors declare that they have no conflict of interest.

References

Chen, Z., Xie, X., Chen, Z. et al. (2025) ‘Classification of red layer desertification scenarios considering the time series statistical characteristics of VIS NIR Spectral Index’, *Transactions of the Chinese Society of Agricultural Engineering*, Vol. 41, No. 9, pp.165–174.

Fan, D., Yang, Z., Li, X. et al. (2025) ‘Cross-feature granularity fusion network for land cover classification of hyperspectral remote sensing images and LiDAR’, *Laser & Optoelectronics Progress*, Vol. 62, No. 10, pp.303–316.

Fayaz, M., Dang, L.M. and Moon, H. (2025) ‘DLAN: a dual attention network for effective land cover classification in remote sensing’, *Knowledge-Based Systems*, Vol. 319, DOI: 10.1016/j.knosys.2025.113620.

Gou, C., Pang, M. and Yang, Y. (2025) 'Improved U-Net convolutional network application for land cover classification in remote sensing images', *Bulletin of Surveying and Mapping*, No. 3, pp.150–155.

Haider, I., Khan, M.A., Masood, S. et al. (2025) 'Performance of pre-trained deep learning models for land use land cover classification using remote sensing imaging datasets', *Environmental Earth Sciences*, Vol. 84, No. 11, pp.1–36, DOI: 10.1007/s12665-025-12317-x.

Li, H., Guo, W., Wu, M. et al. (2025a) 'Visual-language joint representation and intelligent interpretation of remote sensing geo-objects: principles, challenges and opportunities', *Acta Geodaetica et Cartographica Sinica*, Vol. 54, No. 5, pp.853–872.

Li, J., Deng, R., Yan, Y. et al. (2025b) 'Atmospheric correction method of Sentinel-2 data for inland water quality remote sensing', *Remote Sensing Technology and Application*, Vol. 40, No. 2, pp.265–274.

Liu, H. (2024) 'Classification of tree species using UAV-based multi-spectral and multi-seasonal images: a multi-feature-based approach', *New Forests*, Vol. 55, No. 1, pp.173–196, DOI: 10.1007/s11056-023-09974-w.

Liu, K., Xia, L. and Xu, J. (2023) 'An information management system of land resources based on UAV remote sensing', *International Journal of Information and Communication Technology*, Vol. 23, No. 2, pp.107–125, DOI: 10.1504/IJICT.2023.132766.

Liu, X., Li, Y., Zhang, Z. et al. (2025) 'CVS-Net: semantic change detection in remote sensing images using spatial-temporal modeling and edge enhancement', *Journal of Geo-Information Science*, Vol. 27, No. 5, pp.1144–1162.

Ma, Y., Yu, Z., Zhou, Y. et al. (2022) 'UAV system with trinocular vision for external obstacle detection of transmission lines', *Applied Optics*, Vol. 61, No. 12, pp.3297–3311, DOI: 10.1364/AO.446141.

Niu, L., Pan, M., Zhou, Y. et al. (2020) 'Study on optimal urban land classification method based on remote sensing images', *International Journal of Information and Communication Technology*, Vol. 16, No. 4, pp.365–377, DOI: 10.1504/IJICT.2020.107589.

Pacheco, D.G. and de Andrade, A.M. (2024) 'Monitoring agricultural drought using different indices based on remote sensing data in the Brazilian biomes of Cerrado and Atlantic Forest', *International Journal of Biometeorology*, Vol. 68, No. 10, pp.2069–2082, DOI: 10.1007/s00484-024-02731-4.

Qi, K., Ma, X., Jin, Z. et al. (2025) 'Shadow detection method for high-resolution remote sensing images on the basis of shadow direction prior', *National Remote Sensing Bulletin*, Vol. 29, No. 3, pp.776–791.

Sun, K., Xu, Q., Zhang, R. et al. (2025) 'Improved feature pyramid pooling for obstacle extraction in remote sensing images', *Bulletin of Surveying and Mapping*, No. 4, pp.90–95.

Tan, H., Guo, Z., Chen, Y. et al. (2025) 'PV potential analysis through deep learning and remote sensing-based urban land classification', *Applied Energy*, Vol. 387, DOI: 10.1016/j.apenergy.2025.125616.

Tarolli, P., Pijl, A., Cucchiaro, S. et al. (2021) 'Slope instabilities in steep cultivation systems: process classification and opportunities from remote sensing', *Land Degradation & Development*, Vol. 32, No. 3, pp.1368–1388, DOI: 10.1002/ldr.3798.

Turner, K.J., Tzortziou, M. and Grunert, J.S.J. (2022) 'Optical classification of an urbanized estuary using hyperspectral remote sensing reflectance', *Optics Express*, Vol. 30, No. 23, pp.41590–41612, DOI: 10.1364/OE.472765.

Wang, H., Li, X., Huo, L. et al. (2024) 'Global and edge enhanced transformer for semantic segmentation of remote sensing', *Applied Intelligence*, Vol. 54, No. 7, pp.5658–5673, DOI: 10.1007/s10489-024-05457-3.

Wang, X., Liang, W., Bi, C. et al. (2025) 'Classification of hyperspectral remote sensing images by joint hybrid convolution and cascaded group attention mechanisms', *Spectroscopy and Spectral Analysis*, Vol. 45, No. 5, pp.1485–1493.

Wei, R., Wang, L., Wang, T. et al. (2022) 'Segmentation of high-voltage transmission wires from remote sensing images using U-Net with sample generation', *Remote Sensing Letters*, Vol. 13, No. 8, pp.833–843, DOI: 10.1080/2150704X.2022.2089068.

Yang, G., Sun, S., Tian, M. et al. (2025a) 'Building recognition in transmission line corridors based on high-resolution images and improved YOLOv7 model', *Bulletin of Surveying and Mapping*, No. 4, pp.82–89.

Yang, S., He, X., Zhang, T. et al. (2025b) 'Cross-scene remote sensing image classification method based on multi-scale spatial spectral feature alignment', *Science of Surveying and Mapping*, Vol. 50, No. 4, pp.144–158.

Yu, X., Xue, Z., Yang, G. et al. (2024) 'Heterogeneous feature learning network for multimodal remote sensing image collaborative classification', *International Journal of Remote Sensing*, Vol. 45, No. 15, p.26, DOI: 10.1080/01431161.2024.2370502.

Zhang, P.Y. et al. (2025) 'Multi-expert contrastive learning for remote sensing long-tailed image classification', *International Journal of Remote Sensing*, Vol. 46, No. 4, pp.1517–1542, DOI: 10.1080/01431161.2024.2433751.

Zheng, H., Hu, S., Liang, Y. et al. (2024) 'A hidden danger object detection method for transmission line corridor based on YOLO-2MCS', *Transactions of China Electrotechnical Society*, Vol. 39, No. 13, pp.4164–4175.

Zheng, Y., Feng, M., Cai, J. et al. (2025) 'The remote sensing monitoring method of water hyacinth based on geographical spatiotemporal relationship', *Acta Scientiarum Naturalium Universitatis Sunyatseni*, Vol. 64, No. 3, pp.74–82.